Strong magnetic field fluctuations within filamentary auroral density cavities interpreted as VLF saucer sources

D. J. Knudsen,[1,2] R. Kabirzadeh,[1,3] J. K. Burchill,[1] R. F. Pfaff,[2] D. D. Wallis,[4] S. R. Bounds,[5] J. H. Clemmons,[6] and J.-L. Pinçon[7]

[1] The Geoelectrodynamics and Electro-Optical Detection of Electron and Suprathermal Ion Currents (GEODESIC) sounding rocket encountered more than 100 filamentary density cavities associated with enhanced plasma waves at ELF (<3 kHz) and VLF (3–10 kHz) frequencies and at altitudes of 800–990 km during an auroral substorm. These cavities were similar in size (~20 m diameter in most cases) to so-called lower-hybrid cavities (LHCs) observed by previous sounding rockets and satellites; however, in contrast, many of the GEODESIC cavities exhibited up to tenfold enhancements in magnetic wave power throughout the VLF band. GEODESIC also observed enhancements of ELF and VLF electric fields both parallel and perpendicular to the geomagnetic field $\mathbf{B}_0$ within cavities, though the VLF E field increases were often not as large proportionally as seen in the magnetic fields. This behavior is opposite to that predicted by previously published theories of LHCs based on passive scattering of externally incident auroral hiss. We argue that the GEODESIC cavities are active wave generation sites capable of radiating VLF waves into the surrounding plasma and producing VLF saucers, with energy supplied by cold, upward flowing electron beams composing the auroral return current. This interpretation is supported by the observation that the most intense waves, both inside and outside cavities, occurred in regions where energetic electron precipitation was largely inhibited or absent altogether. We suggest that the wave-enhanced cavities encountered by GEODESIC were qualitatively different from those observed by earlier spacecraft because of the fortuitous timing of the GEODESIC launch, which placed the payload at apogee within a substorm-related return current during its most intense phase, lasting only a few minutes.

1. Introduction

[2] Lower-hybrid cavities (LHC), or lower-hybrid solitary structures (LHSS), consist of localized enhancements of wave power near and above the lower-hybrid cutoff frequency. The waves reside in density depletions of several to tens of percent and are sometimes observed to heat ions to several eV [*LaBelle et al.*, 1986; *Kintner et al.*, 1992; *Arnoldy et al.*, 1992; *Vago et al.*, 1992]. These first reports were based on sounding rockets in the topside auroral ionosphere (see review by *Lynch et al.* [1999]). Later, LHSS were observed by the Freja satellite up to 1700 km [*Eriksson et al.*, 1994; *Dovner et al.*, 1994; *Knudsen et al.*, 1998] and on the Cluster satellites throughout the magnetosphere [*Tjulin et al.*, 2003]. The satellite measurements show that LHSS occur in the plasmapause and plasmasphere as well as in the auroral ionosphere. Their formation appears to depend on the presence of ambient VLF hiss of sufficient amplitude [*Lynch et al.*, 1999]. *Høymork et al.* [2000] used chord length distributions to show that LHSS are cylindrical as opposed to planar.

[3] Interferometric analysis of LHSS wave electric fields has demonstrated, on at least three different sounding rockets and on Cluster, that waves above (below) the local lower-hybrid frequency f_{LH} propagate azimuthally in a right- (left-) handed sense around the cavities [*Pinçon et al.*, 1997; *Bonnell et al.*, 1998; *Tjulin et al.*, 2003]. This behavior is consistent with the predictions of a passive scattering model in which linear mode conversion of externally incident whistler mode hiss drives short-wavelength lower-hybrid waves inside cavities [*Seyler*, 1994; *Schuck et al.*, 1998; *Hall et al.*, 2004]. Similar examples of whistler-driven

[1]Department of Physics and Astronomy, University of Calgary, Calgary, Alberta, Canada.
[2]NASA Goddard Space Flight Center, Greenbelt, Maryland, USA.
[3]Department of Electrical Engineering, Stanford University, Stanford, California, USA.
[4]Natural Resources Canada, Ottawa, Ontario, Canada.
[5]Department of Physics and Astronomy, University of Iowa, Iowa City, Iowa, USA.
[6]The Aerospace Corporation, Los Angeles, California, USA.
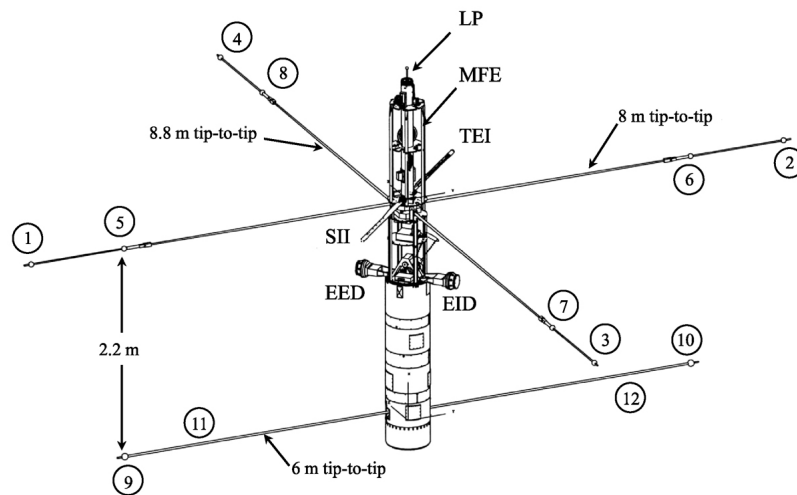[7]LPCE, CNRS, Orléans, France.

Figure 1. Payload configuration, showing the placement of the electric field spheres (numbered), Langmuir probe (LP), search coil antennas (MFE), Suprathermal Electron Imager (SII), Thermal Electron Imager (TEI), and the Energetic Electron and Ion Detectors (EED and EID). The payload was aligned with the geomagnetic field to within 5° throughout most of the flight.

lower-hybrid waves have been observed on density gradients in space [*Bell and Ngo*, 1990, and references therein; *McAdams et al.*, 1998] and in laboratory plasmas [*Bamber et al.*, 1995; *Rosenberg and Gekelman*, 2001]. Search coil magnetometer antennas have been used to confirm that the magnetic component of VLF emissions found in LHSS cavities and on density gradients is usually either absent or small, in general agreement with passive scattering theory [*Vago et al.*, 1992; *Høymork et al.*, 2000; *Reiniusson et al.*, 2006].

[4] *Schuck et al.* [2003] provide a comprehensive review of LHSS. At the time of writing of that review many basic aspects of LHSS were explained as outlined above; however, the cause of the density depletion was a notable exception. Earlier attempts to explain the depletions in terms of pondermotive expulsion along $\mathbf{B}_0$ [*Chang*, 1993; *Shapiro et al.*, 1993] were abandoned when it became apparent that observed wave amplitudes were insufficient to support the observed depletions [*Robinson et al.*, 1996], some as deep as tens of percent [*Kintner et al.*, 1992]. For that reason, LHSS depletions were assumed to be "preexisting" [*Robinson et al.*, 1996; *Schuck et al.*, 2003], meaning they are due to an unspecified mechanism unrelated to the observed lower-hybrid waves and pointing to some additional process that must precede LHC formation. *Knudsen et al.* [2004] showed that density depletions of tens of percent are a natural consequence of ion heating to several eV that is localized on the ion gyroradius scale as observed on several sounding rockets, including Geoelectrodynamics and Electro-Optical Detection of Electron and Suprathermal Ion Currents (GEODESIC).

[5] In this paper we report observations by the GEODESIC sounding rocket of wave-filled cavities very similar to LHCs, but with a strong magnetic field enhancement that is not compatible with the passive scattering model. Moreover, the wave electric fields show none of the mode structure reported by *Pinçon et al.* [1997] and *Tjulin et al.* [2003], indicating that the GEODESIC events are qualitatively different than LHC/LHSS. After describing the GEODESIC experiment and data in sections 2 and 3, we explore and

discuss possible reasons for and the significance of these differences in sections 4 and 5.

2. Experiment

[6] The GEODESIC sounding rocket was launched at 09:19:10.3 UT (00:19:10.3 LT, 22:10 MLT) on 26 February 2000 from Poker Flat Research Range in Alaska. A Black Brant XII vehicle carried the payload to an apogee of 991 km. The payload spin axis was aligned by an attitude control system to within a few degrees of $-\mathbf{B}_0$; the spin period was 5.4 s. Figure 1 shows the configuration of the payload.

[7] GEODESIC carried electron and ion top hat spectrometers (0.01–30 keV), a suprathermal ion imager measuring the range 0–20 eV [see *Burchill et al.*, 2004; *Knudsen et al.*, 2003], a fixed bias cylindrical Langmuir probe in ion saturation, and a swept Langmuir probe to measure electron density and temperature.

[8] Electric fields were measured from DC to 3.5 MHz including broadband time series data and onboard fast Fourier transform power spectra and burst memory "snapshot" collection. For the data shown here, broadband wave data were gathered in a pass band of 0.015–10 kHz (Nyquist) with perpendicular double probes measuring 8.0 and 8.8 m tip to tip, oriented in the plane perpendicular to $\mathbf{B}_0$. Dual sensors on each forward boom provided shorter (1 m) baselines, as shown in Figure 1. An additional pair of booms measuring 6 m tip to tip was deployed 2.2 m aftward, allowing a measurement of electric field components parallel to $\mathbf{B}_0$.

[9] GEODESIC carried two orthogonal induction coil antennas (search coils) sensitive to magnetic perturbations in the plane perpendicular to the payload spin axis, and therefore perpendicular to $\mathbf{B}_0$ to within 5°. Each was 18 cm in diameter with 20,000 turns and contained no magnetic core material. Outputs were sampled at 20,000 s^{-1}. All search coil data presented in this study have been compensated according to a semiempirical response function that accounts for measured values of coil resistance, distributed capacitance and self-inductance. This response (output voltage per unit
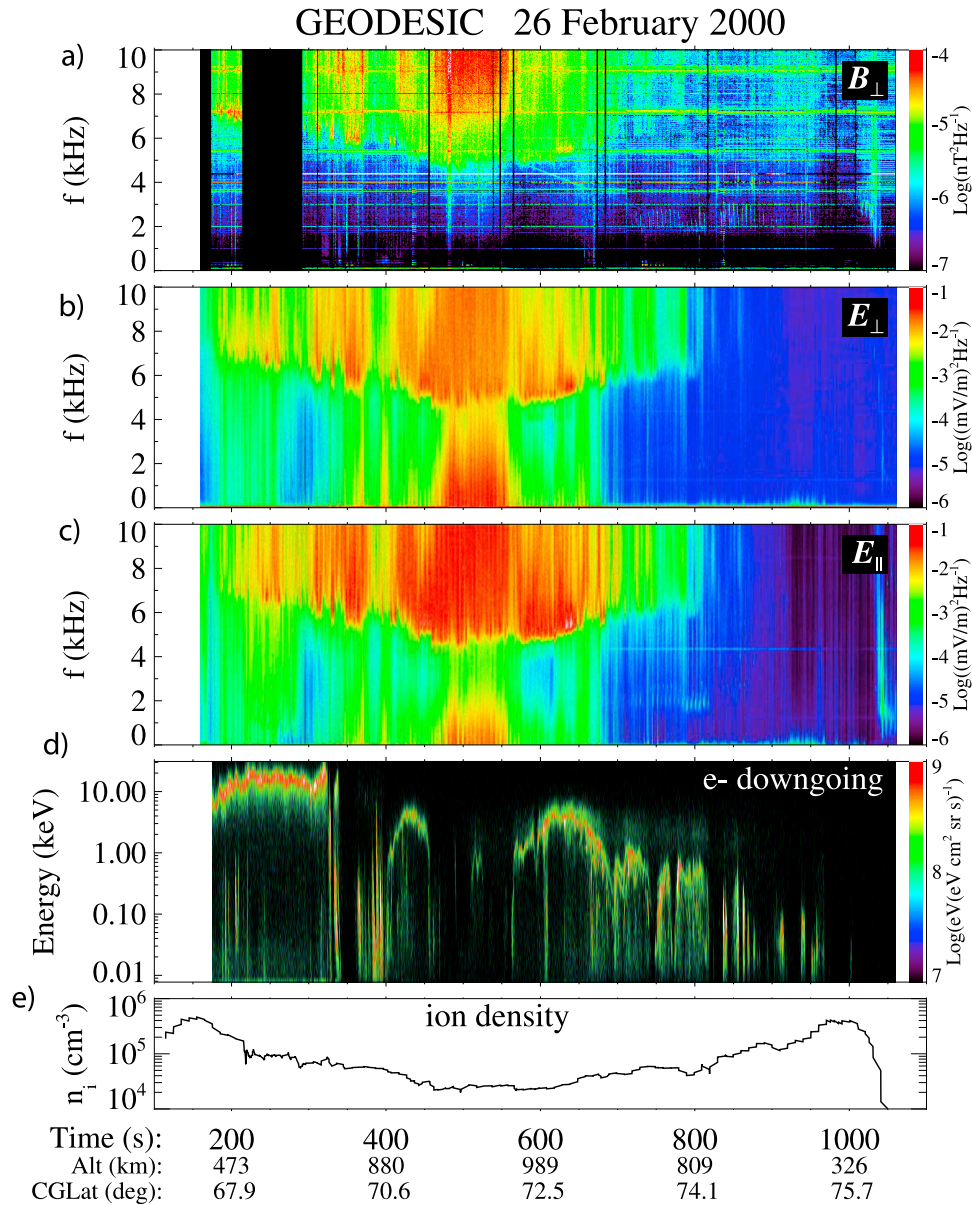
Figure 2. Overview of GEODESIC measurements as a function of time after launch at 09:19:10.3 UT (00:19:10.3 LT), altitude, and corrected geomagnetic latitude (CGLat). (a) $B_\perp$, power spectral density (PSD) measured by a search coil magnetometer sensitive to fluctuations in the plane perpendicular to $\mathbf{B}_0$. (b) $E_\perp$, electric field PSD measured over the short (1 m) "1–5" baseline in the plane perpendicular to $\mathbf{B}_0$. (c) $E_\parallel$, electric field PSD measured parallel to $\mathbf{B}_0$ over the 2.2 m "5–9" baseline. (d) e- downgoing, electron energy flux parallel to $\mathbf{B}_0$. (e) Ion density, as measured from a fixed bias cylindrical Langmuir probe.

input magnetic field) shows a peak near 500 Hz and a monotonic falloff proportional to $1/f^2$ at higher frequencies. In order to prevent contamination from electric fields, the coils (including input terminal pins) were placed inside grounded conductive enclosures.

[10] Postflight analysis of the search coil data revealed an anomalously high degree of correlation between the two orthogonal channels at frequencies above ~1 kHz. The source of this correlation (electronic, inductive) remains unclear. With no physical model of the unwanted coupling, directional field information is compromised. Errors in absolute amplitude due to this coupling are also possible. Nevertheless, we are able to show in section 3 that the coils

clearly respond to magnetic fluctuations of geophysical interest. We are also able to validate the magnetic calibration using expected properties of electromagnetic whistler waves (see section 3.2).

3. Data

3.1. Overview

[11] Figure 2 summarizes the plasma and wave environment through which GEODESIC flew. Starting at Figure 2e, the plasma density during the flight remained high (above $10^4\,\mathrm{cm}^{-3}$) even at the 991 km apogee. Precipitating electrons shown in Figure 2d reach 20 keV within a broad inverted-V
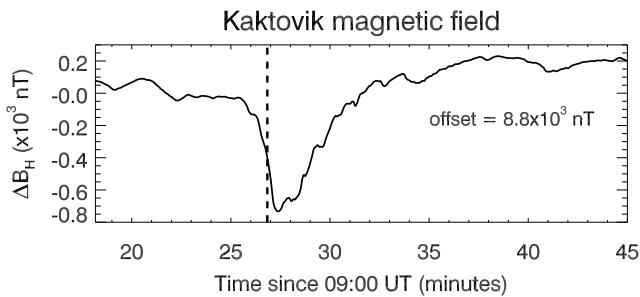
Figure 3. Ground-based magnetometer H (magnetic north) component at Kaktovic, Alaska. The vertical dashed line indicates the time at which GEODESIC was magnetically conjugate. After *Burchill et al.* [2004].

structure in the early portion of the flight. The inverted-V energy rises abruptly just after 300 s, then breaks into softer, energy-dispersed bursts at ~330 s. Measurements at other pitch angles (not shown) demonstrate that these bursts are highly collimated along the magnetic field direction. A second, weak inverted-V is followed by another period with drastically reduced and intermittent downward precipitation lasting from approximately 470 to 570 s, then by a third inverted-V and finally by softer, structured precipitation characteristic of the poleward boundary of the auroral zone in the northern portion of the flight.

[12] Figure 3 shows that the period from ~300–600 s after launch is marked by a strong −750 nT excursion in the H component magnetic field as measured on the ground at Kaktovic, overflown by GEODESIC at ~400 s after launch. Thus, the observed structure in the electron precipitation is strongly affected by the dynamics of a substorm expansion and is at least partly temporal.

[13] Moving up to the electric field data in Figures 2c and 2b, spectrograms of both the perpendicular electric field $E_\perp$ (from baseline 1–5) and parallel electric field $E_\parallel$ (baseline 5–9) are dominated by intense whistler mode auroral hiss with a pronounced lower cutoff between 5 and 7 kHz, easily recognizable as the lower-hybrid frequency f_{LH}. Emissions below f_{LH} are much weaker, with the exception of the period 480–560 s, where intense ELF wave emissions appear. We note that the most intense wave emissions in both the ELF and VLF are found in a region nearly (though not completely) devoid of electron precipitation. Absence of precipitation and strong ELF wave emission are commonly associated with downward current (upgoing electron) regions as identified at higher altitudes [*Paschmann et al.*, 2003]. Furthermore, while failure of the attitude camera precludes an accurate DC magnetic field baseline measurement for GEODESIC, a partial solution (not shown) reveals a system of currents structured on scales of a few kilometers and with both positive and negative excursions of tens of $\mu A\,m^{-2}$. Because of these two observations, we identify the region traversed between 480 and 560 s as a likely site for intense auroral return currents.

[14] Figure 2a demonstrates a significant magnetic component in the VLF hiss as measured by the search coil magnetometer. While there are weak magnetic emissions near and above f_{LH} throughout most of the flight, again the most intense wave emissions coincide with regions nearly devoid of electron precipitation, as in the case of the electric fields.

The magnetic emissions differ qualitatively from the electric fluctuations in that there is no pronounced cutoff at f_{LH}, although the magnetic spectrum intensity does decrease with decreasing frequency. Theoretically, no cutoff is expected, since the lower-hybrid cutoff applies to (essentially) electrostatic lower-hybrid waves propagating nearly perpendicular to $\mathbf{B}_0$, and not to R-O-mode electromagnetic hiss. A second characteristic of the magnetic data is the near absence of any signature from the ELF waves in the downward current region (480–560 s).

[15] We note that noise measured on the launch pad just prior to launch was subtracted from Figure 2a. This included interference lines at frequencies of 4000 and 4375 Hz. We now turn to a study of small-scale wave-filled cavities found within the most intense VLF wave regions shown in Figure 2.

3.2. Wave Cavities

[16] The spectrograms and time series plots in Figure 4 span 2.0 s during the flight at an altitude of 980 km. A strong magnetic interference signal at 4.375 kHz has been suppressed in Figure 4a (top). Five distinct wave cavities are visible, four of which exhibit strong magnetic signatures in both the spectral and time series displays in Figure 4a. The perpendicular electric fields in Figure 4b show clear, broadband responses above the lower-hybrid (LH) cutoff within
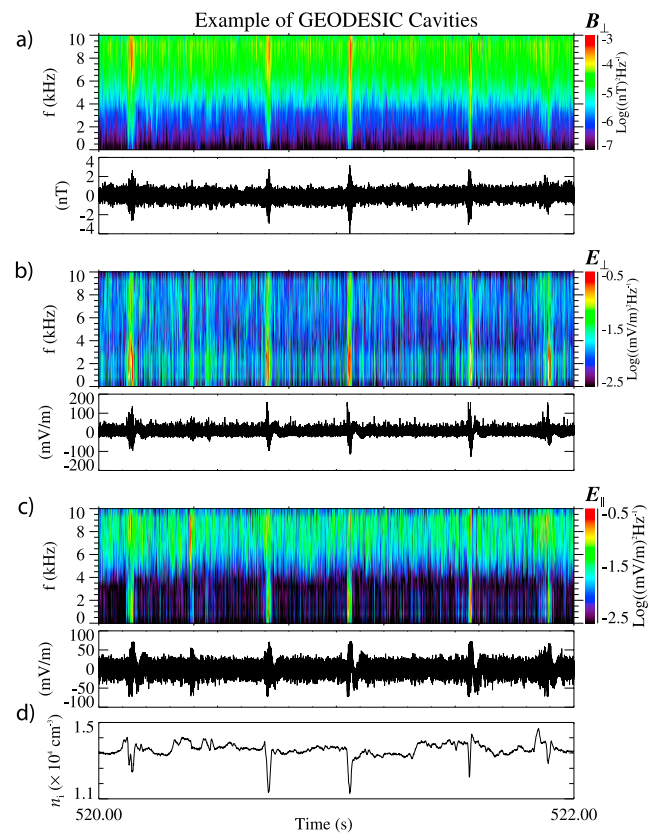

Figure 4. Two-second sequence during the GEODESIC flight showing (a) $B_\perp$, perpendicular magnetic, (b) $E_\perp$, perpendicular electric (baseline 1–5), (c) $E_\parallel$, parallel electric (baseline 5–9), and (d) ion density signatures of ELF/VLF wave cavities. (Note that the density axis does not extend to zero.)
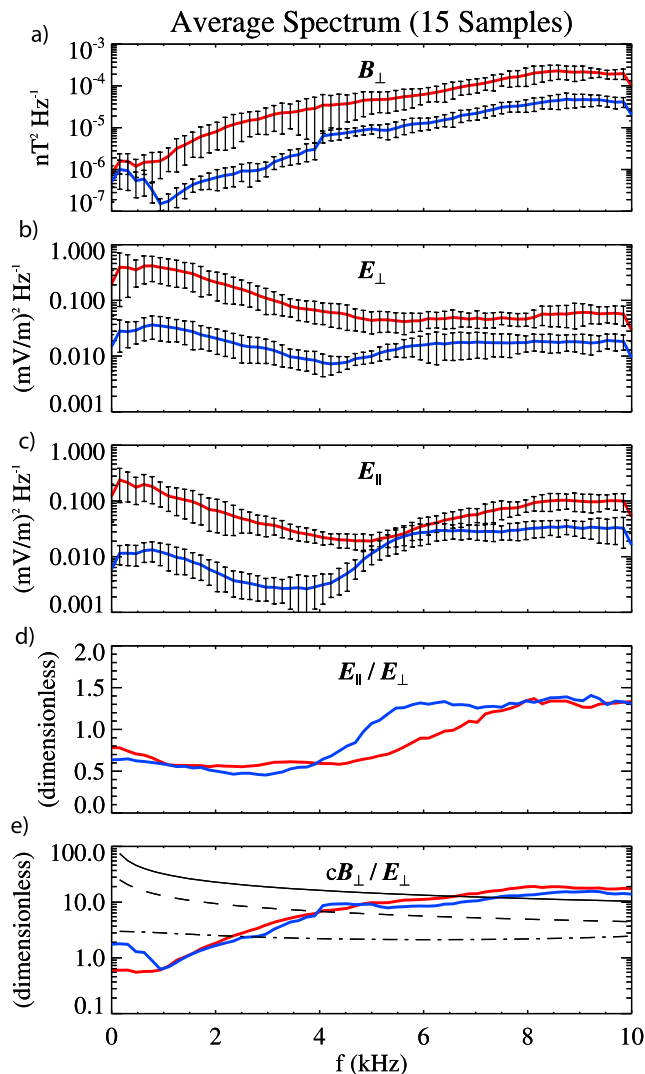
Figure 5. Red lines show power spectra averaged over 15 cavities of field quantities defined in Figure 2. Blue lines are calculated using samples taken outside but adjacent to cavities. Error bars represent RMS variation over the 15 sample spectra. $E_\parallel/E_\perp$ shows the ratio of parallel and perpendicular field amplitudes; $cB_\perp/E_\perp$ is a refractive-index-like quantity. Black lines show the theoretical values for whistler mode waves propagating at 0° (solid), 80° (dashed), and 89° (dot-dashed) with respect to $\mathbf{B_0}$.

cavities, and even stronger signatures in the ELF. In this view the LH cutoff is not very clear even outside cavities; this is because of a strong ELF background in this region.

[17] In contrast, the ELF response is strongly suppressed below f_{LH} in $E_\parallel$ (baseline 5–9). This is expected due to high field-aligned conductivity and is a strong indication that the measurement is, in fact, responding to parallel fields.

[18] The times series of $E_\perp$ in Figure 4b shows that the enhanced fluctuations are superimposed on a perturbation with a timescale of the order of the cavity width (∼20 ms). A high-pass filter at 16 Hz on the channel shown here (VLF 15) has modified the appearance of the features. Inspection of a long-baseline, DC-coupled channel (not shown) shows them to be similar to the bipolar structures reported in

LHCs by *Vago et al.* [1992], who identified them as "payload-generated waves." Using a pair of subpayloads connected by a long tether on the OEDIPUS-C rocket, *Knudsen et al.* [1999] detected bipolar LHC signatures and argued they could be explained by a DC potential of order −0.5 V inside cavities. Regardless of their cause, instrumental or geophysical, the bipolar signature could affect the data only up to a few times the characteristic frequency of the cavities in the payload frame, that is, of the order of 100–200 Hz. In the data shown in Figure 4, electric field intensities extend smoothly from tens of hertz all the way to 10 kHz. Apart from the possibility of payload-generated waves at the lowest end of this range, the ELF waves in the GEODESIC data appear to be geophysical.

[19] Figure 4e shows plasma densities derived from a fixed bias Langmuir probe biased to −5 V. The depletion depths of the cavities shown here are of order 10%. A study of these depletions and a mechanism that can generate them is given by *Knudsen et al.* [2004]. Cavity widths based on ions, plasma density, and electric fields were reported by *Burchill et al.* [2004], who identified 106 events in total.

3.3. Cavity Wave Spectra

[20] Figure 5 shows average spectra calculated from 15 cavities having the strongest magnetic field intensities. Each panel compares average spectra measured inside these cavities (in red) with spectra taken adjacent to them, 0.1 s away (in blue). Figure 5a shows that the average magnetic field power spectral density increases monotonically with frequency, with no discernible feature near f_{LH}. (Points near 4.375 kHz suffered from strong interference and were discarded and replaced with interpolated values.) The spectrum from cavity interiors has the same shape as that taken outside, but is 5–10 times more intense.

[21] Figures 5b and 5c show averaged spectra of $E_\perp$ and $E_\parallel$ from the 1–5 and 5–9 baselines, respectively. The spectrum of the ambient $E_\perp$ outside cavities (in blue) is almost flat and exhibits only a slight depression just below the cutoff frequency (5 kHz). Inside cavities, the $E_\perp$ power spectral density (PSD) increases tenfold below f_{LH}, and threefold to fivefold above, with no signature of the f_{LH} cutoff. Presumably this cutoff is obscured by the intense ELF waves extending up to f_{LH} [see also *Burchill et al.*, 2004, Figure 7].

[22] Unlike the case for $E_\perp$, the average $E_\parallel$ spectrum outside cavities is strongly attenuated below f_{LH}. Inside cavities the emissions are again even more intense below f_{LH} than above, and the average spectrum inside is similar to that of $E_\perp$, though somewhat reduced. This is illustrated in Figure 5d for "$E_\parallel/E_\perp$," showing a nearly constant spectral ratio of between 0.5 and 0.8 within cavities and a ratio of unity outside cavities and above f_{LH}.

[23] Figure 5e plots the refractive-index-like ratio $cB_\perp/E_\perp$. Normally, we would wish to compare components of $E_\perp$ and $B_\perp$ that are perpendicular to each other as well as to $\mathbf{B_0}$. But as discussed in section 2, orthogonal magnetic field channels appear to be coupled. This fact leads to uncertainties both in the direction and absolute amplitude of the magnetic fluctuations. Nevertheless, using single-channel calibration values determined prior to launch, Figure 5 shows that the ratio $cB_\perp/E_\perp$ falls within the theoretical refractive index for whistler mode hiss [*Stix*, 1992] propagating parallel to $\mathbf{B_0}$ (solid black line.) This provides an independent check that

the magnetic calibration is reasonable to within a factor of ~2.

[24] Inside cavities and above 1 kHz, the ratio $cB_\perp/E_\perp$ is nearly equal to or slightly higher than its value outside cavities, on average. This result is independent of the absolute accuracy of the field measurements and depends instead only on their linearity.

[25] As shown by the dashed lines in Figure 5e, whistler mode waves propagating nearly perpendicular to $\mathbf{B}_0$ have a much smaller refractive index than measured either inside or outside the cavities. Since any waves localized within cavities must have a highly oblique wave vector, the whistler mode is not a viable candidate to explain the magnetic field enhancements associated with cavities.

4. Interpretation

[26] GEODESIC's detections of large magnetic enhancements are in marked contrast to all earlier observations, raising the question of their origin. In this section we explore an interpretation in which the field enhancements seen by GEODESIC were the result not of coupling to externally incident waves but instead were generated within the cavities themselves. We propose that unstable auroral return currents produce electrostatic waves having electric field components both perpendicular and parallel to $\mathbf{B}_0$. Fluctuating parallel electric fields then modulate the parallel current, leading to strong magnetic fluctuations.

[27] A full description of the cavity fields shown in Figure 4 would require not only frequency but also wave number spectra that are simply not possible to obtain from a rapidly moving spacecraft that traverses the highly structured cavities in only ~20 ms and that can introduce significant Doppler shifts. This situation severely limits any theoretical description since the perpendicular ion response to wave fields depends strongly on wavelength and also on ion composition. On the other hand, the parallel response, being dominated by electron currents, is much simpler, especially in the case of the very low β plasma relevant to GEODESIC. (β is the ratio of particle to magnetic pressure.) In this section we exploit this fact to arrive at simple and testable predictions relating perpendicular magnetic and parallel electric field fluctuations.

4.1. Source of Fluctuating B

[28] Assuming cylindrical symmetry, the Maxwell-Ampère relation can be used to relate the average field-aligned current $j_\parallel$ over a circular cross section of radius R to the average perpendicular (azimuthal) magnetic field around its perimeter:

$$B_\perp = \frac{R}{2}\left(\mu_0 j_\parallel + \frac{1}{c^2}\frac{\partial E_\parallel}{\partial t}\right) \qquad (1)$$

Referring to Figure 5a, the magnetic fluctuations in the 5–10 kHz range have an RMS amplitude of the order of 0.7 nT $[(10^{-4}\ \mathrm{nT}^2\ \mathrm{Hz}^{-1}) \times (5000\ \mathrm{Hz})]^{-1/2}$. Ignoring the displacement current on the right-hand side of equation (1), a magnetic field of this magnitude will result from a fluctuating field-aligned current having an RMS amplitude of ~140 μA m^{-2} over a 20 m diameter cylinder. Such a current could result, for example, from 20% of the background electron

population (with a density of 10^4 cm^{-3}) being accelerated to only 0.5 eV in the direction parallel to $\mathbf{B}_0$.

[29] Next we take into account the first-order dynamics of field-aligned electron motion by separating parallel electron velocity and electron density into background plus fluctuating components: $v_{e,\parallel} = v_{e,\parallel,0} + \delta v_{e,\parallel}$; $n_e = n_{e,0} + \delta n_e$. Field-aligned electron motion responds to a fluctuating parallel electric field $\delta E_\parallel$ according to the parallel momentum equation

$$\left(\frac{\partial}{\partial t} + v_{e,\parallel,0}\frac{\partial}{\partial \parallel}\right)\delta v_{e,\parallel} = \frac{q_e}{m_e}\delta E_\parallel \qquad (2)$$

The field-aligned current is carried primarily by electrons: $j_\parallel = q_e n_e v_{e,\parallel}$. The first-order fluctuating current is

$$\delta j_\parallel = q_e\left(n_{e,0}\delta v_{e,\parallel} + \delta n_e v_{e,\parallel,0}\right) \qquad (3)$$

[30] The fluctuating density and velocity are related by the continuity equation, $\partial n_e/\partial t + \partial(n_e v_{e,\parallel})/\partial \parallel = 0$. Assuming $\exp(i\omega t - ik_\parallel z)$ dependence (z is the field-aligned coordinate),

$$\delta n_e = \frac{k_\parallel n_{e,0}\delta v_{e,\parallel}}{\omega - k_\parallel v_{e,\parallel,0}} \qquad (4)$$

Finally, combining equations (1)–(4),

$$\frac{cB_\perp}{\delta E_\parallel} = \frac{i\pi R}{cf}\left(\frac{f_{pe}^2}{\left(1 - v_{e,\parallel,0}/v_{ph,\parallel}\right)^2} - f^2\right) \qquad (5)$$

where f_{pe} is the electron plasma frequency, $v_{ph,\parallel} = \omega/k_\parallel$, c is the speed of light, and R is the radius of the current filament. The last term in (5) is due to parallel displacement current, and in this form can be seen to be less important than parallel conduction current by a factor of $f_{pe}^2/f^2 = 10^4$ at 10 kHz for a density of 10^4 cm^{-3}.

[31] Using observed values for $n_{e,0}$ and R (10 m), the ratio $v_{e,\parallel,0}/v_{ph,\parallel}$ is the only free parameter. Assuming an electron beam moving at four times its thermal speed ($v_{e,\parallel,0} = 4v_{th,e}$), parallel wavelength $\lambda_\parallel$ becomes the adjustable parameter. Figure 6 compares measured values of $|cB_\perp/\delta E_\parallel|$ with equation (5) for various values of $\lambda_\parallel$, and shows that measured values are consistent with $\lambda_\parallel \sim 40$–80 m over most of the spectrum, with a possible second branch of solution for longer wavelengths that could apply at the higher frequencies. Although this range of $\lambda_\parallel$ is not verified independently, such wavelengths are plausible.

[32] An additional test of the plausibility of this model comes from recognizing that if the magnetic fluctuations seen by GEODESIC are indeed due to fluctuating field-aligned currents confined within cylindrical density depletions, one would expect magnetic field intensity to be zero in the cavity centers. GEODESIC did not fly directly through cavity centers in general, and so one would not expect to find zero (or even minimum) δB in all crossings. However, some of the events do indeed exhibit a local minimum in magnetic wave power near their centers. Figure 7 shows an example as seen in a magnetic field intensity profile and wavelet spectrum, along with electric field intensity profiles using four different baselines. The differences in the electric field profiles are due
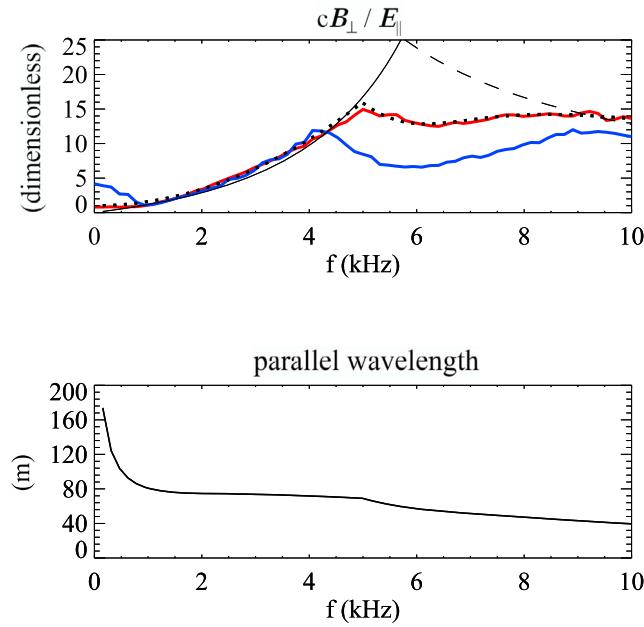
$cB_\perp / E_\parallel$

parallel wavelength

Figure 6. (top) Refractive-index-like quantity (equation (5)) based on perpendicular magnetic and parallel electric fields averaged over 15 spectra measured inside (red) and outside (blue) cavities. The solid black line plots equation (5) for cavity radius R = 10 m, an electron beam velocity 4 times its thermal speed, a beam temperature of 0.1 eV, and parallel wavelength $\lambda_\parallel$ = 70 m. The dotted black line is an approximate fit of equation (5) to the measured values obtained by adjusting $\lambda_\parallel$. (bottom) The resulting parallel wavelength spectrum. The dashed black line in Figure 6 (top) illustrates a second branch of solution for a parallel phase velocity exceeding the electron beam velocity, in this case for $\lambda_\parallel$ = 1000 m.

to the fact that they sampled different cross sections of the cavity.

[33] As noted, the simple model presented here does not include particle motion or currents perpendicular to $\mathbf{B}_0$, and therefore cannot describe a normal mode of the plasma. In particular, the magnetic fields predicted by this model should not be interpreted as the magnetic signature of whistler mode waves. Instead, the model provides a testable relation between two observables in the near field of an oscillating current filament driven by electrostatic waves having an electric field component parallel to $\mathbf{B}_0$. Calculating the coupling of these oscillations to whistler waves in the surrounding plasma would require a more complete plasma model that is beyond the scope of this study.

4.2. Source of Fluctuating $E_\parallel$

[34] *James* [1976] argued that saucer-shaped VLF wave signatures are driven by electrostatic waves arising from a cold-electron drift instability in downward current regions. We extend this scenario one step further to say that parallel electric fields associated with the electrostatic waves modulate the current-carrying beam and also drive any ambient electrons along $\mathbf{B}$, generating a magnetic signature. Such a mixture of ambient (nondrifting) and beam electrons will occur when beam electrons are accelerated below the point of

Table 1. Input Parameters for WHAMP Wave Growth Calculations

Species	Mass (H+)	Charge (q_{e^+})	Density (cm^{-3})	Temp (eV)	$V_{\parallel\, drift}$ ($V_{th,j}$)
Ions (O+)	15.9281	+1	14×10^3	0.2	0.0
Electrons	0.0	−1	7–12.6×10^3	0.2	0.0
Electron beam	0.0	−1	1.4–7×10^3	0.05–0.5	2.0–7.0

observation. The lower boundaries of density cavities are possible regions of such acceleration. Because field-aligned current must be conserved, the drop in density as electrons enter cavities must be compensated by increased upward velocity.

[35] To test the feasibility of this wave generation mechanism for GEODESIC, we estimate electrostatic wave growth rates for GEODESIC conditions using the WHAMP dispersion solver [*Rönnmark*, 1985], which assumes infinite plane waves in a homogeneous plasma. These assumptions clearly do not hold for the GEODESIC cavities. However, the density cavities are of the order of a full perpendicular wavelength in diameter, and in the absence of a more representative model we believe that WHAMP's estimates are valid in an order-of-magnitude sense, and are useful for establishing trends.
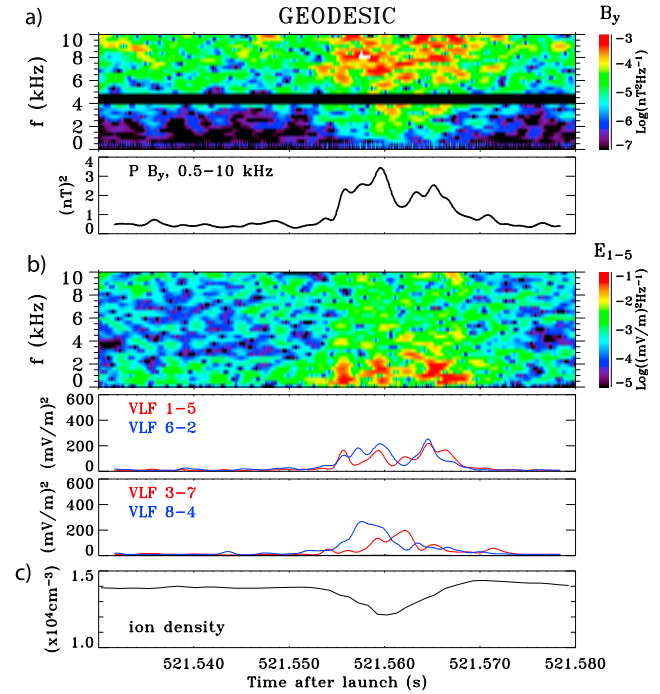

Figure 7. (a) Wavelet spectrogram and integrated power profile of magnetic fluctuations $B_\perp$ across a single cavity, showing a minimum near the center. (b) Similar displays for electric fields obtained from the four 1 m long baselines perpendicular to $\mathbf{B}_0$. "VLF" indicates that these electric field channels are AC-coupled with a filter cutoff near the Nyqvist frequency of 10 kHz. (c) Ion density from the fixed bias Langmuir probe. The dark strip in Figure 7a (top) is due to suppression of a strong interference signal originating on the payload.
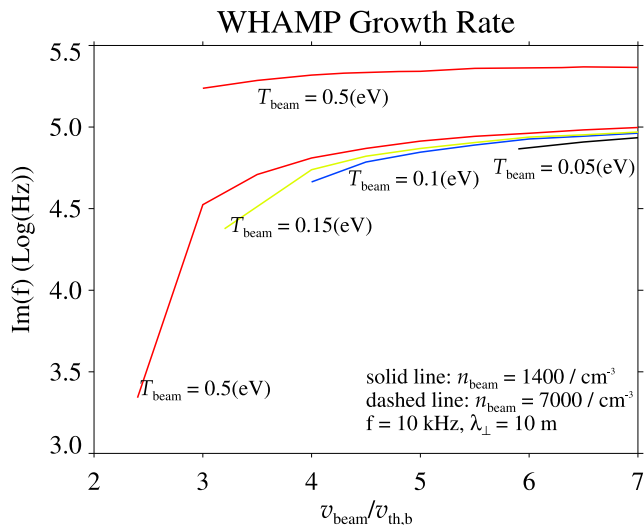
Figure 8. Wave growth rates calculated from WHAMP for a variety of electron beam densities and temperatures, assuming a background density of 10^4 cm^{-3} and a perpendicular wavelength of 10 m.

Figure 10. Dependence of electrostatic wave growth rate on relative beam density for parameters given in Table 1, supporting the idea that depletions in background density can enhance wave growth.

[36] Table 1 shows assumed parameters of the ambient plasma and the electron beam. Figure 8 shows strong wave growth for beam velocities of only a few times the electron thermal speed, a condition that is presumably easy to meet within a strongly driven ionospheric return current, as it implies electron energies of the order of only 1 eV or even less. Figure 9 illustrates that the drift of cold, current-carrying electrons can reasonably lead to parallel electric fields that are comparable to or even larger than perpendicular fields for wave numbers and other parameters typical of the GEODESIC environment. This is consistent with Figure 5d, which shows that $E_\perp > E_\parallel$ near the lower-hybrid frequency as expected, and the two components become comparable at higher frequencies.

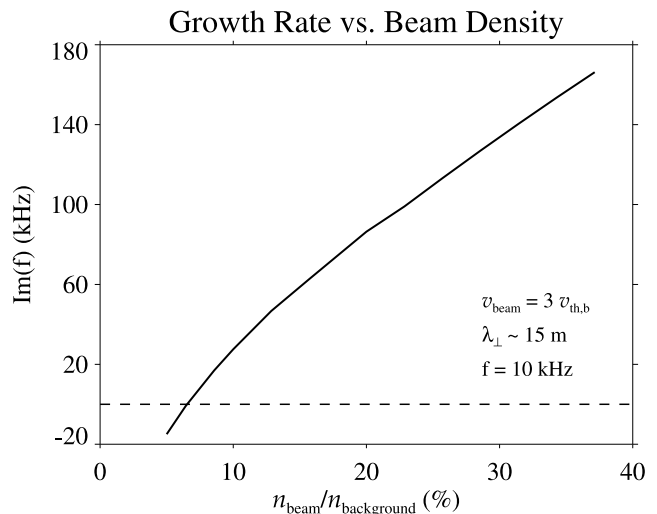[37] The argument above offers an explanation of the source of the strong waves observed by GEODESIC, but not the cause of their localization. Figure 10 shows the dependence of the linear wave growth rate as a function of beam-to-ambient electron density as determined by WHAMP. For the same amount of DC field-aligned current, growth rate rises sharply as background density decreases. This suggests that fields both parallel and perpendicular to $\mathbf{B}_0$ will grow preferentially in regions of locally depressed density. As shown by *Knudsen et al.* [2004], locally enhanced perpendicular electric fields can enlarge ion gyro-orbits through heating so as to decrease time-averaged plasma density in the higher-field region. Since this depleted density can enhance instability according to Figure 10, a feedback loop can result, favoring density-depleted structures localized on the scale of the heated ion gyroradii, of order 10 m. A self-consistent analysis of this mechanism is beyond the scope of this study; however, the simple model shows that localized ion heating to a few eV as seen on GEODESIC [*Burchill et al.*, 2004] can easily produce
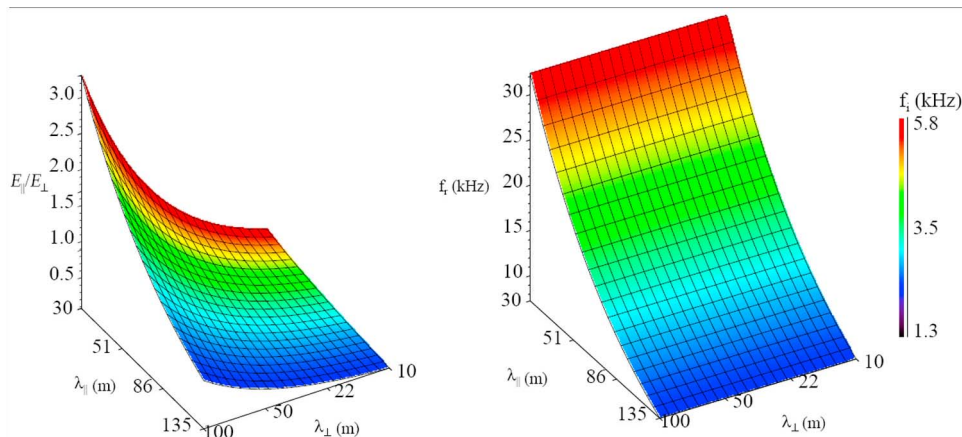

Figure 9. Electrostatic wave growth rates (color scale) in a homogenous plasma for parameters given in Table 1. (left) Growth rate f_i of 10 kHz waves showing strong growth of waves having $\lambda_\perp = 10$ m, $\lambda_\parallel \sim 100$ m, with corresponding values of $|E_z/E_x| = |E_\parallel/E_\perp| \geq 1$. (right) Wave growth rate as a function of real frequency f_r, $\lambda_\perp$, and $\lambda_\parallel$.

localized density depletions of the order of 10% [*Knudsen et al.*, 2004].

5. Discussion and Conclusions

[38] The GEODESIC sounding rocket measured strong magnetic field fluctuations inside localized density cavities in the auroral ionosphere. Previous searches found that the magnetic component is either absent or weak [*Vago et al.*, 1992; *Høymork et al.*, 2000; *Reiniusson et al.*, 2006].

[39] In considering why GEODESIC found such a difference, the most likely explanation has to do with the geophysical environment. Whereas previous rocket-measured LHCs were found in or near auroral arcs, most of the GEODESIC events were found in a region of strongly reduced electron precipitation and highly structured and intense field-aligned currents, that is, a region in which intense auroral return currents are likely to be found. The magnetogram shown in Figure 3 is a signature of a substorm-related auroral electrojet and is not a direct measure of a return current, but it does indicate the presence of very intense ionospheric currents in the brief period during which GEODESIC passed over Kaktovic, on the north coast of Alaska.

[40] In addition to the strong VLF magnetic fields, a second indication that the GEODESIC wave cavities are qualitatively different from those reported previously is the lack of the telltale counterrotating eigenmode structure seen in frequency-wave number spectra of electric fields measured by the AMICIST sounding rocket [*Pinçon et al.*, 1997; *Bonnell et al.*, 1998]. This was determined by processing fields from several of the clearest GEODESIC events using the same procedure and software that were developed for the AMICIST rocket. This absence of resonant mode structure is consistent with a strong driving source within cavities.

[41] Yet another unique aspect of the GEODESIC measurements is the high plasma density ($\sim 10^4$ cm^{-3}) near apogee, 1 to 2 orders of magnitude higher than is typically observed in the nighttime topside ionosphere. In the interpretation that electrostatic waves drive ambient electrons parallel to $\mathbf{B}_0$, the amplitude of the resulting magnetic fluctuations is proportional to electron density. It is conceivable that previous missions flew through wave generation regions having lower plasma density and therefore undetectable magnetic enhancements.

[42] Strong parallel electric fields have been reported from the FAST satellite at higher altitudes [*Ergun et al.*, 2001], also in return current regions. High time resolution waveform snapshots on FAST show that both parallel and perpendicular electric field enhancements are due to discrete, charged "phase-space holes" traveling with the electron beam. GEODESIC waveform measurements were not able to resolve such structures; however, it is possible that the low-frequency E field signatures seen by GEODESIC are also the result of phase-space holes, which might be interpreted as the nonlinearly saturated state of the linearly unstable wave modes characterized by Figures 8 and 9.

5.1. Measurement Anomalies and Uncertainties

[43] As described in section 2, GEODESIC carried two orthogonal search coil antennas in order to determine the polarization of the magnetic waves in the plane perpendicular to $\mathbf{B}_0$. However, the two components exhibit an anomalously high degree of correlation at frequencies above 1 kHz, indicating an unwanted coupling of unknown origin and rendering polarization measurements unreliable. Coupling between the two channels will also affect amplitude measurements, though a simple model (namely, a cross-sensor coupling factor of less than unity) suggests errors of a factor of two or less. This level of uncertainty is adequate to support the conclusions of this study.

[44] The parallel electric field measurements summarized in Figures 2 and 4 are new and unusual. While parallel electric fields in return current regions are both predicted by theory and observed, at least at higher (FAST) altitudes, Figure 2 shows significant wave power in $E_\parallel$ throughout the flight. Pickup of perpendicular fields due to imperfect alignment with **B** is not a viable explanation since GEODESIC was aligned to within 5° throughout most of the flight, and the parallel component is comparable to and often stronger than $E_\perp$, at least above the lower-hybrid cutoff frequency. Also, as illustrated in Figure 5, the shape of the perpendicular and parallel spectra are markedly different, meaning one channel cannot be explained simply through cross coupling with another. Improper boom deployment is also unlikely since perpendicular electric fields measured by the forward and aft boom sets agree well with each other. Finally, we note that our conclusions depend only on $E_\parallel$ enhancements within cavities embedded in return current regions, and that an explanation of all aspects of the measurements shown in Figure 2 is beyond the scope of this study.

[45] Regardless of the above issues and uncertainties, confidence in both $B_\perp$ and $E_\parallel$ measurements is enhanced considerably by the fact that together they are consistent with each other through a simple physical model of field-aligned current-carrying electrons driven by $E_\parallel$ within cavities.

5.2. Relation to VLF Saucers

[46] VLF saucers are V-shaped features in frequency-time spectrograms observed by satellites over a wide range of altitudes [*Gurnett and Frank*, 1972; *Lönnqvist et al.*, 1993]. Using ray tracing, *James* [1976, p. 514] inferred typical source dimensions of "0.5 km horizontally by no more than 10 km vertically." The total radiant power is of the order of 10 mW, and the source spectrum is flat within a few decibels from 100 Hz to 20 kHz. James argued that saucers are driven by superthermal electrons with energies less than 5 eV which destabilize electrostatic waves as assumed in section 4 of this paper.

[47] Using the FAST satellite, *Ergun et al.* [2003] established that most but not all saucer sources are embedded in regions of downward current/upward electrons. In that study the upgoing (downgoing) electron variants had energies above (below) 10 eV. They demonstrated that saucers are, in fact, composed of many individual "point sources" distributed in altitude and more confined in latitude than in longitude. *Ergun et al.* [2001] also reported a strong correlation between the occurrence of saucers and electron phase space holes.

[48] The altitude of the GEODESIC wave events, their location within a region in which auroral return currents are likely to occur, their highly localized nature, their relatively flat field spectra and the evidence that they are active sources

of VLF wave power are all consistent with these earlier reports of saucer source properties. Furthermore, the VLF power available within the GEODESIC cavities is sufficient to account for the *James* [1976] estimate of 10 mW for total radiant power. This can be seen by taking the product of a typical parallel electric field of 20 mV m^{-1} (0.1 (mV m^{-1})^2 Hz^{-1} over a bandwidth of 5 kHz, see Figure 5) and typical field-aligned current fluctuations of 140 μA m^{-2} (see section 4), resulting in over 800 mW of power available within a 20 m diameter, kilometer long cavity. A radiation efficiency of even 1% results in a total radiant power of the order of 10 mW as reported by *James* [1976].

[49] It would be preferable to observe directly a saucer resulting from the GEODESIC events; however, this would require a second, simultaneous observation far above the source. On the other hand, it is conceivable that some dispersion might be visible from waves originating from within a single cavity a few km below GEODESIC's trajectory; this was investigated in detail by *Kabirzadeh* [2010], and while highly localized saucer-shaped signatures were visible around events such as those shown in Figure 4, data processing artifacts could not be ruled out as an alternative explanation, and the results were inconclusive.

[50] The results of this paper are as follows:

1. GEODESIC sounding rocket observations show several-fold increases in VLF magnetic field amplitude localized within filamentary density depletions of the order of 1–10%.

2. VLF electric field amplitudes both perpendicular and parallel to $\mathbf{B}_0$ are also enhanced within the cavities, though on average the fractional increase is not as large as for magnetic fields. This observation excludes an interpretation in terms of lower-hybrid waves driven by linear coupling to externally incident whistler mode hiss as developed in previous studies of LHSS.

3. Observed magnetic field amplitudes perpendicular to $\mathbf{B}_0$ are consistent with an interpretation in which filamentary field-aligned currents were carried by electrons whose velocities were modulated by the observed parallel electric fields.

4. VLF and ELF electric fluctuations are consistent with an interpretation in terms of filaments of unstable auroral return current carried by cold ionospheric electrons.

5. The magnetic wave-filled cavities are found at altitudes between 800 and 990 km, within a region where downward electron precipitation is strongly reduced, and at the time of the most intense few minutes of an auroral substorm expansion as indicated by a −750 nT deflection of the magnetic *H* component as measured on the ground.

6. A wavelet analysis identical to that used on data from previous sounding rockets and satellites (not shown here) shows no evidence for counterrotating eigenmodes, and therefore for passive scattering, supporting the conclusion that GEODESIC cavity waves were not passively scattered from waves originating outside cavities but instead were driven locally.

7. The altitude, degree of structure, likely association with regions of auroral return current, spectral shape, and total power of the wave-filled cavities are consistent with properties of VLF saucer source regions reported previously [*James*, 1976; *Ergun et al.* 2003].

[51] In summary, our results support a model of localized ELF/VLF wave cavities in which intense auroral return currents become unstable to electrostatic wave growth in the ELF/VLF frequency range when thermal electron flow becomes supersonic; these waves can energize ions and cause density depletions localized on scales comparable to heated ion gyro radii according to the mechanism reported by *Knudsen et al.* [2004]. The depleted density destabilizes the waves further, expelling still more ions and leading to stable filamentary cavities. Fluctuating electric fields parallel to the geomagnetic field then drive electron currents parallel to $\mathbf{B}_0$; these currents in turn generate magnetic oscillations as observed by GEODESIC. The fluctuating current filaments can radiate waves which disperse over large distances to form VLF saucers. When the intensity of the auroral return current diminishes, density cavities formed during the actively driven phase can persist and act as resonators for lower-hybrid waves excited by externally incident auroral hiss emissions, resulting in the passive lower-hybrid wave-filled cavities observed and described in previous studies.

References

Arnoldy, R. L., K. A. Lynch, P. M. Kintner, J. Vago, S. Chesney, T. E. Moore, and C. J. Pollock (1992), Bursts of transverse ion acceleration at rocket altitudes, *Geophys. Res. Lett.*, *19*, 413.

Bamber, J. F., J. E. Maggs, and W. Gekelman (1995), Whistler wave interaction with a density striation: A laboratory investigation of an auroral process, *J. Geophys. Res.*, *100*, 23,795.

Bell, T. F., and H. D. Ngo (1990), Electrostatic lower hybrid waves excited by electromagnetic whistler mode waves scattering from planar magnetic-field-aligned plasma density irregularities, *J. Geophys. Res.*, *95*, 149.

Bonnell, J. W., P. W. Schuck, J.-L. Pinçon, C. E. Seyler, and P. M. Kintner (1998), Observation of bound states and counterrotating lower hybrid eigenmodes in the auroral ionosphere, *Phys. Rev. Lett.*, *80*, 5734, doi:10.1103/PhysRevLett.80.5734.

Burchill, J. K., D. J. Knudsen, B. J. J. Bock, R. F. Pfaff Jr., D. D. Wallis, J. H. Clemmons, S. R. Bounds, and H. Stenbaek-Nielsen (2004), Core ion interactions with BB ELF, lower hybrid, and Alfvén waves in the high-latitude topside ionosphere, *J. Geophys. Res.*, *109*, A01219, doi:10.1029/2003JA010073.

Chang, T. (1993), Lower hybrid collapse, caviton turbulence, and charged particle energization in the topside auroral ionosphere and magnetosphere, *Phys. Fluids B*, *5*, 2646.

Dovner, P. O., A. I. Eriksson, R. Boström, and B. Holback (1994), Freja multiprobe observations of electrostatic solitary structures, *Geophys. Res. Lett.*, *21*, 1827.

Ergun, R. E., C. W. Carlson, J. P. McFadden, R. J. Strangeway, M. V. Goldman, and D. L. Newman (2001) Electron phase-space holes and the VLF saucer source region, *Geophys. Res. Lett.*, *28*, 3805.

Ergun, R. E., C. Carlson, J. McFadden, R. Strangeway, M. Goldman, and D. Newman (2003), Fast auroral snapshot observations of very low frequency saucers, *Phys. Plasmas*, *10*, 454, doi:10.1063/1.1530160.

Eriksson, A. I., B. Holback, P. O. Dovner, R. Boström, G. Holmgren, M. André, L. Eliasson, and P. M. Kintner (1994), Freja observations of correlated small-scale density depletions and enhanced lower hybrid waves, *Geophys. Res. Lett.*, *21*, 1843.

Gurnett, D. A., and L. A. Frank (1972), VLF hiss and related plasma observations in the polar magnetosphere, *J. Geophys. Res.*, *77*, 172.

Hall, J. O., A. I. Eriksson, and T. B. Leyser (2004), Excitation of localized rotating waves in plasma density cavities by scattering of fast magnetosonic waves, *Phys. Rev. Lett.*, *92*, 255002.

Høymork, S., H. L. Pécseli, B. Lybekk, J. Trulsen, and A. Eriksson (2000), Cavitation of lower hybrid waves in the Earth's ionosphere: A model analysis, *J. Geophys. Res.*, *105*, 18,519.

James, H. G. (1976), VLF saucers, *J. Geophys. Res.*, *81*, 501, doi:10.1029/JA081i004p00501.

Kabirzadeh, R. (2010), Electromagnetic wave-filled cavities observed by the GEODESIC sounding rocket: A direct encounter with VLF saucer source regions, M.Sc. thesis, Univ. of Calgary, Calgary, Alberta, Canada.

Kintner, P. M., J. Vago, S. Chesney, R. L. Arnoldy, K. A. Lynch, C. J. Pollock, and T. E. Moore (1992), Localized lower hybrid acceleration of ionospheric plasma, *Phys. Rev. Lett.*, *68*, 2448.

Knudsen, D. J., P. O. Dovner, A. I. Eriksson, and K. A. Lynch (1998), Effect of lower hybrid cavities on core plasma observed by Freja, *J. Geophys. Res.*, *103*(A3), 4241–4249, doi:10.1029/97JA01993.

Knudsen, D. J., D. D. Wallis, and H. G. James (1999), Tethered two-point measurements of solitary auroral density cavities, *Geophys. Res. Lett.*, *26*, 2933.

Knudsen, D. J., J. K. Burchill, K. Berg, T. Cameron, G. A. Enno, E. P. King, C. G. Marcellus, I. Wevers, and R. A. King (2003), A low-energy charged particle distribution imager with a compact sensor for space applications, *Rev. Sci. Instrum.*, *74*, 202.

Knudsen, D. J., et al. (2004), Lower-hybrid cavity density depletions as a result of transverse ion acceleration localized on the gyroradius scale, *J. Geophys. Res.*, *109*, A04212, doi:10.1029/2003JA010089.

LaBelle, J. P. M. Kintner, A. W. Yau, and B. A. Whalen (1986), Large amplitude wave packets observed in the ionosphere in association with transverse ion acceleration, *J. Geophys. Res.*, *91*, 7113.

Lönnqvist, H., M. André, L. Matson, A. Bahnsen, L. G. Blomberg, and R. E. Erlandson (1993), Generation of VLF saucer emissions observed by the Viking satellite, *J. Geophys. Res.*, *98*, 13,565.

Lynch, K. A., R. L. Arnoldy, P. M. Kintner, P. Schuck, J. W. Bonnell, and V. Coffey (1999), Auroral ion acceleration from lower hybrid solitary structures: A summary of sounding rocket observations, *J. Geophys. Res.*, *104*, 28,515.

McAdams, K. L., J. LaBelle, P. W. Schuck, and P. M. Kintner (1998), PHAZE II observations of lower hybrid burst structures occurring on density gradients, *Geophys. Res. Lett.*, *25*, 3091.

Paschmann, G., S. Haaland, and R. Treumann (Eds.) (2003), *Auroral Plasma Physics*, *Space Sci. Ser. ISSI*, vol. 15, 500 pp., Kluwer, Dordrecht, Netherlands.

Pinçon, J. L., P. M. Kintner, P. W. Schuck, and C. E. Seyler (1997), Observation and analysis of lower hybrid solitary structures as rotating eigenmodes, *J. Geophys. Res.*, *102*, 17,283.

Reiniusson, A., G. Stenberg, P. Norqvist, A. I. Eriksson, and K. Rönnmark (2006), Enhancement of electric and magnetic wave fields at density gradients, *Ann. Geophys.*, *24*, 367.

Robinson, P. A., A. Melatos, and W. Rozmus (1996), Is there lower-hybrid collapse at auroral latitudes?: Theory versus observations, *J. Geophys. Res.*, *101*, 21,545.

Rönnmark, K. G. (1985), Kinetic theory of plasma waves, *Space Sci. Rev.*, *42*, 411, doi:10.1007/BF00214996.

Rosenberg, S., and W. Gekelman (2001), A three-dimensional experimental study of lower hybrid wave interactions with field-aligned density depletions, *J. Geophys. Res.*, *106*, 28,867.

Schuck, P. W., C. E. Seyler, J.-L. Pinçon, J. W. Bonnell, and P. M. Kintner (1998), Theory, simulation, and observation of discrete eigenmodes associated with lower hybrid solitary structures, *J. Geophys. Res.*, *103*, 6935.

Schuck, P. W., J. W. Bonnell, and P. M. Kintner (2003), A review of lower hybrid solitary structures, *IEEE Trans. Plasma Sci.*, *31*, 1125.

Seyler, C. E. (1994), Lower hybrid wave phenomena associated with density depletions, *J. Geophys. Res.*, *99*, 19,513.

Shapiro, B. D., V. I. Shevchenko, G. I. Solov'ev, V. P. Kalinin, R. Bingham, R. Z. Sagdeev, M. Ashour-Abdalla, J. Dawson, and J. J. Su (1993), Wave collapse at the lower-hybrid resonance, *Phys. Fluids B*, *5*, 3148.

Stix, T. H. (1992), *Waves in Plasmas*, Am. Inst. of Phys., College Park, Md.

Tjulin A., A. I. Eriksson, and M. André (2003), Lower hybrid cavities in the inner magnetosphere, *Geophys. Res. Lett.*, *30*(7), 1364, doi:10.1029/2003GL016915.

Vago, J. L., P. M. Kintner, S. W. Chesney, R. L. Arnoldy, K. A. Lynch, T. E. Moore, and C. J. Pollock (1992), Transverse ion acceleration by localized lower hybrid waves in the topside auroral ionosphere, *J. Geophys. Res.*, *97*, 16,935.

S. R. Bounds, Department of Physics and Astronomy, University of Iowa, 516 Van Allen Hall, Iowa City, IA 52242, USA.

J. K. Burchill and D. J. Knudsen, Department of Physics and Astronomy, University of Calgary, 2500 University Dr., N.W., Calgary, AB T2N 1N4, Canada. (knudsen@ucalgary.ca; burchill@phys.ucalgary.ca)

J. H. Clemmons, The Aerospace Corporation, Mail Stop M2/260, PO Box 92957, Los Angeles, CA 90009-2957, USA.

R. Kabirzadeh, Department of Electrical Engineering, Stanford University, Stanford, CA 94305-7609, USA.

R. F. Pfaff, NASA Goddard Space Flight Center, Mail Code 696, Greenbelt, MD 20771, USA.

J.-L. Pinçon, LPC2E, CNRS, 3A, Av. de la Recherce Scientifique, F-45071 Orléans CEDEX 2, France.

D. D. Wallis, Natural Resources Canada, 2617 Anderson Rd., Ottawa, ON K1A 0Y3, Canada.